

1     **The formation and geometry characteristics of boulder bars due to**  
2     **outburst flood triggered by the overtopped landslide dam failure**

3     Xiangang Jiang<sup>✉1</sup> · Haiguang Cheng<sup>1</sup> · Lei Gao<sup>2</sup> · Weiming Liu<sup>3</sup>

4     <sup>1</sup>College of Civil Engineering, Sichuan Agricultural University, Dujiangyan, Chengdu 611830,  
5     China

6     <sup>2</sup>Key Laboratory of Ministry of Education for Geomechanics and Embankment Engineering,  
7     Hohai University, Nanjing 210098, China

8     <sup>3</sup>Key Laboratory of Mountain Hazards and Earth Surface Process, Institute of Mountain Hazards  
9     and Environment, Chinese Academy of Sciences, Chengdu 610041, China

10    Correspondence to: Xiangang Jiang (✉E-mail: [jxgjim@163.com](mailto:jxgjim@163.com))

11    **Abstract**

12    Boulder bars are a common form of riverbed morphology that could be affected by  
13    landslide dams. However, few studies have focused on the formation and geometry  
14    characteristics of boulder bars due to outburst floods triggered by landslide dam failure.  
15    In such way, eight group landslide dam failure experiments with movable bed length  
16    for 4 to 7 times of dam length with 25 boulder bars were carried out. In addition, 38  
17    boulder bars formed in the **field** triggered by four landslide dam failures were  
18    investigated. The aim of this paper is to study the formation and geometry  
19    characteristics of boulder bars along the riverbeds. The results show that boulder bars  
20    are formed after peak discharge of outburst flow. The number of boulder bars is 0.4 to  
21    1.0 times the ratio of river bed length to dam bottom length. Besides, boulder bars have  
22    the characteristic of lengthening towards upstream during the failure process. Boulder

23 bar's upstream edge has a more extensive development than boulder bar downstream  
24 edge. The length of a boulder bar along the channel changes faster than the boulder  
25 bar's width and height. After the dam failure, the boulder bar's length is about 8 to 14  
26 times of width. The relationship between ratio of boulder bar length to width and  
27 boulder bar's dimensionless length could be described with a hyperbolic equation. The  
28 dimensionless area of boulder bar increases linearly with the dimensionless area of the  
29 river section, and the linear ratio is about 0.5. With the field data, it demonstrates the  
30 formation and geometry characteristics of boulder bars in tests are consistent with the  
31 field boulder bars. Therefore, the results in this paper are credible, and can be applied  
32 to the river bed's geomorphological characteristics analysis triggered by overtopped  
33 landslide dam failure. The plenty of experimental and field data could contribute to the  
34 community for the boulder bars' research.

### 35 **Keywords**

36 Landslide dam · Overtopping failure · Boulder bar · Formation and geometry  
37 characteristics

## 38 **1. Introduction**

39 Activities such as rainfalls and earthquakes often cause landslides, which block  
40 the river to form a water-retaining body similar to a reservoir dam, called a landslide  
41 dam (Takahashi, 2007; Costa and Schuster, 1988; Casagli, 2003). According to  
42 statistics, 85 % of the dams failed within one year after formations, and more than 50 %  
43 of the dams breached with overtopping mode (Costa and Schuster, 1988). When the

44 dam breach, the storage water erupt and flown carrying the dam materials to the  
45 downstream riverbed, which may change original riverbed geomorphology.

46 Many studies on the influence of flood geomorphology and sedimentary  
47 characteristics have proved that the outburst flood energy is huge, and it can entrain and  
48 transport materials of various sizes, from clay to boulders. A large number of boulders  
49 gather in the river to form bars, namely boulder bars. The downstream riverbed's  
50 geomorphology will be significantly affected and undergo significant changes (Lamb  
51 and Fonstad, 2010; Maizels, 1997; Russell and Knudsen, 1999; Marren and Schuh,  
52 2009; Benito and O'Connor, 2003; Carling, 2013; Wu et al., 2020). Boulder bars are  
53 one common landform formed during the outburst flood evolution (Turzewski et al.,  
54 2019; Jiang and Wei, 2020; Wu et al., 2020). For example, in the 2000 year, Yigong  
55 outburst flood, due to its huge lake storage, formed many huge boulder bars on the river  
56 bed. The boulder bars had a significant impact on the development of the river bedform.  
57 And Wu et al. (2020) investigated the impact of this event on river morphology and  
58 analyzed the shapes and geometric characteristics of the boulder bars caused by the  
59 overtopping flood. And they found that the boulder bar components are poorly sorted.  
60 Turzewski et al. (2019) studied the particle gradation of the boulder bars during the  
61 Yigong River landslide dam failure process. They found that the boulder bars' particle  
62 sizes decrease along the lower reaches of the river bed. But they did not analyze the  
63 evolution characteristics of boulder bar's size in detail. Lamb and Fonstad (2010)  
64 suggested that the rising and falling stages of the outburst flood had a greater impact on  
65 riverbed geomorphology and analyzed the characteristics of the median diameter of

66 material in boulder bar.

67 The boulder bars triggered by landslide dam failure are formed under a  
68 nonequilibrium sediment transport condition. Sediment pulses delivered to downstream  
69 are dispersive under this **condition**. It is very different from river dunes under steady  
70 flow conditions, which is an equilibrium sediments transport condition, and the  
71 sandbars maintain their geometry when they migrate downstream. It means that the  
72 boulder bars' shape and geometry size are variation during its formation process.  
73 Furthermore, the formation of boulder bars is different from sandbars which formed by  
74 translative depositional processes (Mohrig and Smith, 1996; Ashworth et al., 2000;  
75 Shaw and McElroy, 2016).

76 Because lack of investigations about the growth characteristics of boulder bars  
77 during the landslide dam failure process in the field, some researchers had conducted  
78 landslide dam failure experiments in the lab (Ashworth, 1996; Jiang and Wei, 2020).  
79 Ashworth (1996) used flume experiments to study the boulder bar's growth. However,  
80 in their **experiments**, the inflow conditions are quite different from the outburst flood.  
81 Therefore, the research results' applicability to the boulder bar formed by the outburst  
82 flood remains uncertain. Jiang and Wei (2020) qualitatively analyzed the formation  
83 process of boulder bar in the evolution of overtopping outburst floods using dam failure  
84 experiments and initially discussed the characteristics of geometric size of boulder bars  
85 after dam failure. However, the characteristics of the boulder bar's distribution and  
86 geometric size characteristics during the dam failure process have not been analyzed.

87 Above all, there is a common academic consensus that outburst flow triggered by

88 landslide dam failure could change the geomorphology of downstream riverbed.  
89 Although, the failure process of the dam and the hydraulic characteristics of the outburst  
90 flood, such the characteristics of breaching hydraulic graph, erosion rate and peak  
91 discharge (Morris et al., 2009; Jiang and Wei 2018; Jiang, 2019), are clear, the impact  
92 of the outburst flood triggered by landslide dam failure on the geomorphology of the  
93 downstream riverbed during the failure process and after failure is still lack of research.  
94 Boulder bar is the substance occurred during the dam failure process which is an  
95 indicator for the variation of riverbed geomorphology. What are the formation  
96 characteristics of boulder bars during the dam failure process? And what geometry  
97 characteristics of boulder bar are during the dam failure process and after the dam  
98 failure? These questions are still not clear and should be answered. Understanding these  
99 questions is helpful for predication of riverbed landform influenced by landslide dam  
100 failure, and benefit to assessment of stream restoration and river navigation.

101 This paper focuses on the formation processes and the geometrical size  
102 characteristics of boulder bars in the downstream channel during and after the  
103 overtopping failure process. Firstly, through flume experiments, boulder bars' formation  
104 processes on the downstream channel under the dammed lake failure condition were  
105 reproduced. Then, based on the experimental data, the development characteristics of  
106 boulder bars' upstream and downstream edges were analyzed. Furthermore, statistical  
107 analysis of boulder bars geometrical sizes at each moment during and after the failure  
108 process, such as length, width, height, volume and area of boulder bar, had been carried  
109 out to obtain boulder bars' size characteristics. Finally, compare the distribution and

110 geometry characteristics of the boulder bar formed in the experiment and field to verify  
 111 experiment results' reliability. The results can be applied to the river bed's  
 112 geomorphological characteristics research affected by the outburst flood triggered by  
 113 landslide dam failure. And also, this paper provides a large number of experimental and  
 114 field boulder bars' data reference to the analysis of the erosion and accumulation  
 115 characteristics of the downstream river channel.

## 116 **2. Experimental design**

### 117 **2.1 Model design and experimental materials**

118 The longitudinal profiles of experimental landslide dams were trapezoidal and  
 119 triangular. The trapezoidal dam height and crest width were both 0.3 m, and the  
 120 triangular dam height was also 0.3 m. In the experiment, river bed slope angle  $\theta$  was  
 121 fixed at  $10^\circ$ , and the landslide dam upstream slope angle  $\alpha$  was set to  $40^\circ$ , and the  
 122 landslide dam downstream slope angles  $\beta$  were set to five different values. The  
 123 moveable bed was set downstream of the model dam, which had a length of 8 m. The  
 124 downstream channel bed's length was about 4 to 7 times of dam length along the  
 125 channel. The test parameters are shown in Table 1.

126 **Table 1** test parameters

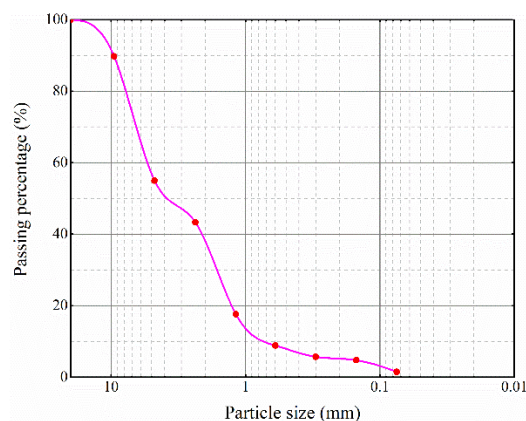
No.	Dam shape	$\beta$ ( $^\circ$ )
T1	Trapezoid	10
T2	Trapezoid	15
T3	Trapezoid	20
T4	Trapezoid	25
T5	Trapezoid	30
T6	Tringle	10
T7	Tringle	15
T8	Tringle	20

127 Peng and Zhang (2012) proposed that landslide dam height ( $H_d$ ), dam bottom  
128 width parallel to the channel ( $W_d$ ), dam volume ( $V_d$ ), and reservoir volume ( $V_l$ ) are the  
129 key geometric parameters of landslide dam, and proposed a set of dimensionless  
130 numbers,  $\frac{H_d}{W_d}$ ,  $\frac{V_d^{1/3}}{H_d}$  and  $\frac{V_l^{1/3}}{H_d}$ , to verify whether the established dam model is  
131 consistent with the landslide dam in the field (Zhou et al., 2019). As the field data show  
132 that the  $\frac{H_d}{W_d}$ ,  $\frac{V_d^{1/3}}{H_d}$  and  $\frac{V_l^{1/3}}{H_d}$  are ranged about 0.001 to 2, 0 to 40, and 0 to 20 for  
133 filed landslide dam (Zhou et al., 2019). Table 2 shows the dimensionless numbers of  
134 the experimental dams, which are all within the acceptable range of the field landslide  
135 dams, indicating that the dams in the experiments are relatively close to field landslide  
136 dams.  
137 **Table 2** landslide dam parameters. The value of  $\frac{H_d}{W_d}$  ranges from 0.1 to 0.3, and  $\frac{V_d^{1/3}}{H_d}$  and  $\frac{V_l^{1/3}}{H_d}$   
138 both range from 1 to 2, which all fall within the acceptable range of values of the field landslide  
139 dams (Zhou et al., 2019).

No.	$H_d$ (m)	$W_d$ (m)	$\frac{H_d}{W_d}$	$\frac{V_d^{1/3}}{H_d}$	$\frac{V_l^{1/3}}{H_d}$
T1	0.3	2.359	0.127	1.643	1.477
T2	0.3	1.777	0.169	1.513	1.477
T3	0.3	1.482	0.202	1.437	1.477
T4	0.3	1.301	0.231	1.387	1.477
T5	0.3	1.177	0.255	1.350	1.477
T6	0.3	2.059	0.146	1.508	1.477
T7	0.3	1.477	0.203	1.350	1.477
T8	0.3	1.182	0.254	1.254	1.477

140 In the field, the landslide dam and the boulder bars are almost consisted of  
141 mixtures. The dam materials used in this study were mixtures of sand and gravels.  
142 Considering the grain size effect and the flume space limitation, the maximum sediment  
143 particle size was set to 20 mm. The materials used in the tests had a median particle

144 size of  $D_{50} = 3.8$  mm. A dimensionless parameter measure of the spread in the grain-size  
145 distribution,  $\sigma_g = d_{90}/d_{10} = 14.3$  represents a wide grain size range of granular materials  
146 for landslide dams. While the materials of riverbed are different from that of landslide  
147 dam, it is hard to find a general description of the difference. Thus, we designed the  
148 materials of riverbed and landslide dam the same for present experiments. Moreover,  
149 the compositions of field dam and riverbed can be heterogeneous, i.e. the distribution  
150 of coarse particle within landslide dam is inhomogeneity, there is still no quantitative  
151 representation of the heterogeneity. Therefore, the coarse particles and fines were mixed  
152 uniform, which means the distribution of coarse particles were homogeneous. The  
153 channel morphology in nature is complex and diverse, which was not considered in the  
154 experiments. Instead, a straight, aequate and flat channel was set, which is helpful to  
155 reveal the fundamental mechanism of the formation process and geometric  
156 characteristics of boulder bars. The thickness of the riverbed was set to 0.06 m. The  
157 gradation curve of material particles' sizes is shown in Fig. 1.



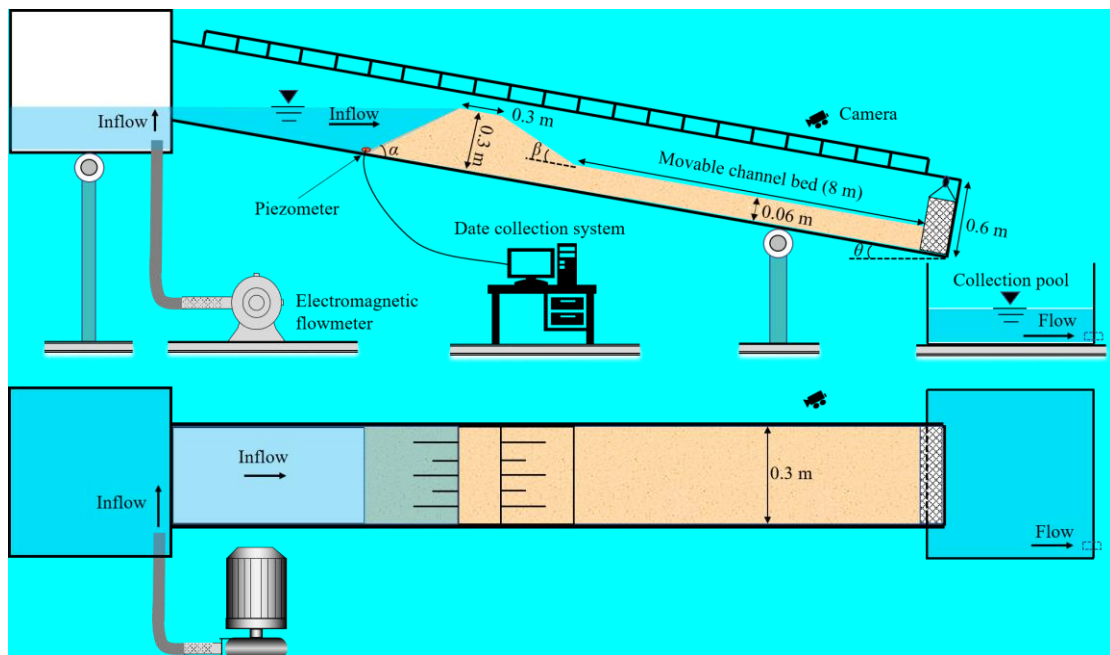
158 **Figure 1.** Gradation curve of the dam materials  
159

## 160 2.2 Experimental apparatus

161 The experimental setups are shown in Fig. 2. The flume was 15 m long, 0.3 m



162 wide, and 0.6 m high. The flume slope was adjustable from 10 to 30°. One side of the  
 163 flume was transparent glass, and scale lines were drawn on the glass to facilitate  
 164 observation and recording of experimental phenomena. The inflow discharge upstream  
 165 the dam was set as  $1.0 \text{ L s}^{-1}$ . Under the control of the electromagnetic flowmeter, the  
 166 error range could be controlled within  $\pm 0.01 \text{ L s}^{-1}$ . During the tests, the toe of the dam  
 167 upstream slope was set at 4.5 m away from the water supply tank. A baffle with a height  
 168 of 6 cm was set at the flume end as a boundary condition. Seven cameras were placed  
 169 on the transparent glass side of the flume, one camera was placed on the top of the dam,  
 170 and one camera was placed directly behind the flume. A total of nine cameras recorded  
 171 the whole experimental phenomena.



172  
 173 **Figure 2.** Experimental setups. (a) Front view of the flume. (b) Top view of the flume.

174 **2.3 Measurements**

175 In the experiment, using the scale lines on the transparent glass on the side of the  
 176 flume, we can accurately read the boulder bars' positions at each moment. Boulder bars'

177 lengths, widths, and heights could be obtained from the screen. According to the actual  
178 boulder bars' geometric characteristics, the boulder bars were divided into several parts,  
179 and then the volume calculation formula of the similar geometric body was used to  
180 calculate the volume of each part respectively, and finally, the boulder bars' volumes  
181 were obtained by summing. The method of obtaining the boulder bar area was the same  
182 as that of the volume. After the dam was completely failed, we collected all the boulder  
183 bar materials. Then dried and screened silt to obtain the boulder bar material gradation  
184 information.

### 185 **3. Experimental results**

#### 186 **3.1 Formation processes of boulder bars**

187 The formation processes of boulder bars are almost similar for all the tests.  
188 Therefore, it takes the T7 test as an example to analyze below in this section, as shown  
189 in Fig. 3. When the flow overtopped the dam crest, the outburst flood carried the dam  
190 materials to the dam downstream slope (T=5 s) and then to the channel bed (T=19 s)  
191 with outburst flow discharge increasing. It should be noted that although a large number  
192 of sediments were transported on the channel bed before the peak discharge, no boulder  
193 bar formed on the downstream channel bed. After the moment of peak discharge, the  
194 flow discharge gradually weakened, and dam materials were transported to the position  
195 near the dam toe. The flow could not transport all the sediments away, and some  
196 sediments gradually silted down, then the first boulder bar occurred near the dam toe  
197 (T=30 s, the boulder bar in the figure is marked with a blue dotted line). After the first

198 boulder bar was formed, the flow direction was changed when water flow bypassed the  
199 boulder bar. And the moving sediments still moved along the original direction due to  
200 inertia, which causes sediments piled up to form the second boulder bar on the opposite  
201 side of the first boulder bar (T=33s).

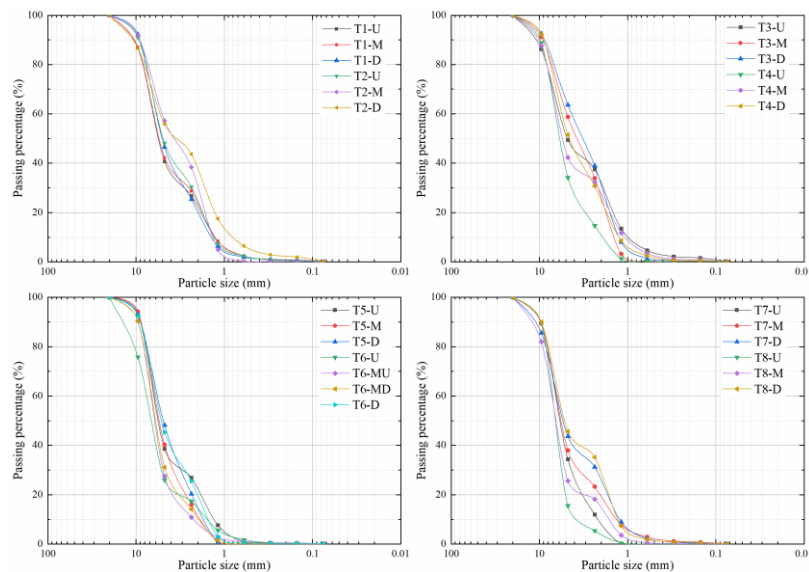
202 Similarly, the first and second boulder bars affected the formation of the boulder  
203 bar downstream. Eventually, boulder bars were scattered on both sides of the channel,  
204 forming a meandering channel downstream (T=40 and 47 s). This phenomenon is in  
205 good agreement with the field boulder bars along the Yigong river (Wu et al., 2020). In  
206 addition, the Froude number of flows on the downstream were all larger than 2.5 during  
207 the bars' formation process, indicating these bars were formed in a supercritical flow  
208 (diffusive) condition. It suggests that boulder bars were formed on dispersive sediment  
209 pulses which delivered from the upstream during the landslide dam failure process.  
210 (Shaw and McElroy, 2016).



211  
212 **Figure. 3.** The riverbed morphology at six different moments during the boulder bars' formations  
213 and growths process for the T7 experiment. The boulder bars in the figure are marked with blue  
214 dotted lines.

215 Turzewski et al. (2019) measured the sizes of field boulder bars. They found that

216 grain sizes of boulder bars decrease downstream. In this experiment, sediments in  
 217 boulder bars after dam failure from different locations were collected. After sieving the  
 218 sediments, the gradation curves of the materials were obtained as shown in Fig. 4. The  
 219 figures show that the contents of fines in the compositions become much less and their  
 220 mean diameters become larger than the initial sediments. It means that in the boulder  
 221 bars coarse sediment tends to comprise much of the bar material. Meanwhile, the figure  
 222 indicates that as the distance between the boulder bar and the dam increases, the particle  
 223 diameter in the bars shows a decreasing trend. This feature is consistent with the  
 224 description of Turzewski et al. (2019).



225  
 226 **Figure 4.** Gradation curve of the boulder bar materials. Notation: U, M, D, MU, and MD, represent  
 227 the boulder bar near the upstream reaches, the boulder bar near the middle reaches, the boulder bar  
 228 near the downstream reaches, the boulder bar near the middle-upstream reaches, and the boulder  
 229 bar near the middle-downstream reaches, respectively.

230

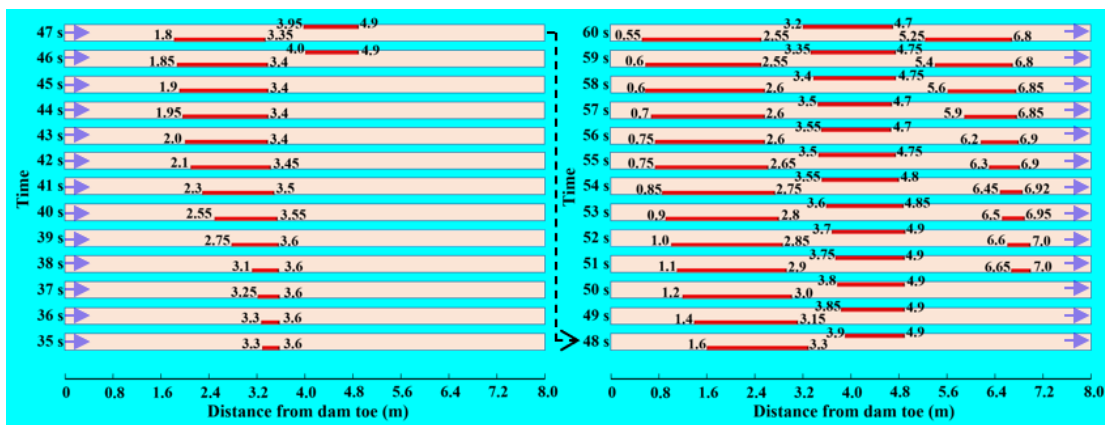
### 231 3.2 Evolution characteristics of the boulder bars during dam failure process

232 Figure. 5 shows boulder bars' locations on the channel bed during the dam failure

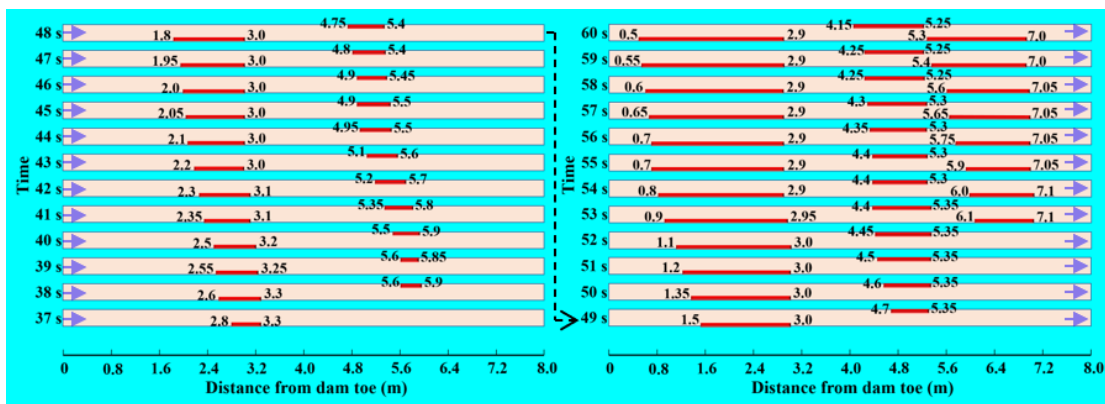
233 process. The red lines in the figure represent the boulder bars' outlines, and the orange  
234 rectangles represent the channels. It clearly shows the formation sequences of boulder  
235 bars at different locations. That is, boulder bars were formed first near the dams  
236 (upstream reaches of riverbed), and the farther from the dam toe, the later the boulder  
237 bar was formed, which is consistent with the content of Sect. 3.1. Boulder bars near the  
238 downstream dam toes are all located on the dam breach side across the river. This  
239 characteristic has also been found in Chen et al. (2015).

240 According to the boulder bars' formation sequences, the channel bed's boulder bars  
241 were divided into three types: I. the boulder bar near the upstream reaches, that is, the  
242 boulder bar near the dam toe; II. the boulder bar at the middle reaches; and III. the  
243 boulder bar near the downstream reaches. Figure 5 shows that the upstream edges of  
244 the boulder bars of type I for all the tests basically moved toward the dams with time  
245 development. The movement directions of the downstream edges of boulder bars of  
246 type I showed a little different: for T1, T2 and T5, the boulder bars' downstream edges  
247 moved toward the dam toes, from a distance from the downstream toe of 3.6 to 2.55 m,  
248 3.3 to 2.9 m and 3.7 to 3.4 m, respectively, as shown in Fig.5 (a), (b) and (e); for T6,  
249 T7, and T8, the boulder bars' downstream edges first moved away from the dam toes  
250 and then moved toward the dam toes, and the downstream edges move forward  
251 compared to the original location. However, the distance they moved is 0.1 to 0.2 m, as  
252 shown in Fig.5 (f), (g), and (h); for T3 and T4, the boulder bars' downstream edges  
253 positions remained almost unchanged, see Fig.5(c) and (d). No matter how the  
254 downstream edge positions of the boulder bars type I changed, there is a common

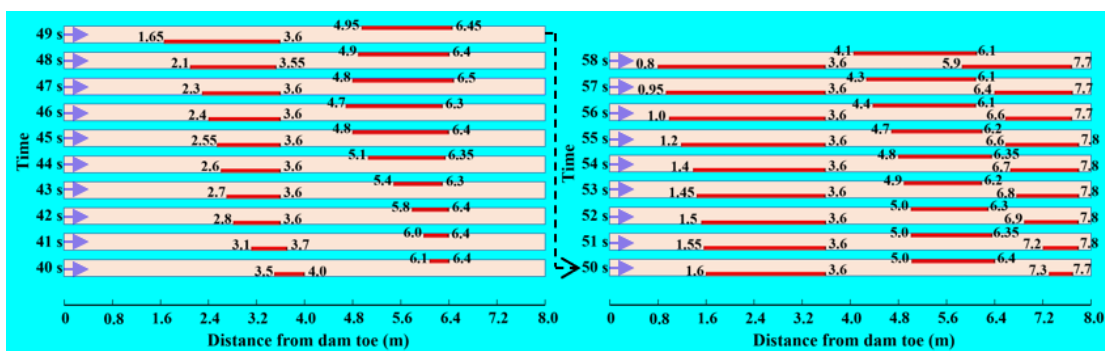
255 feature: compared with the initial positions of the boulder bars, the downstream edges  
 256 almost remained original locations, and the movement distances were much smaller  
 257 than those of boulder bars' upstream edges. The lengths of the boulder bars of type I  
 258 increased with the failure time. It can be seen that the sediments on the boulder bars'  
 259 upstream edges played a great role in the length developments of type I boulder bars.



(a)



(b)



(c)

260

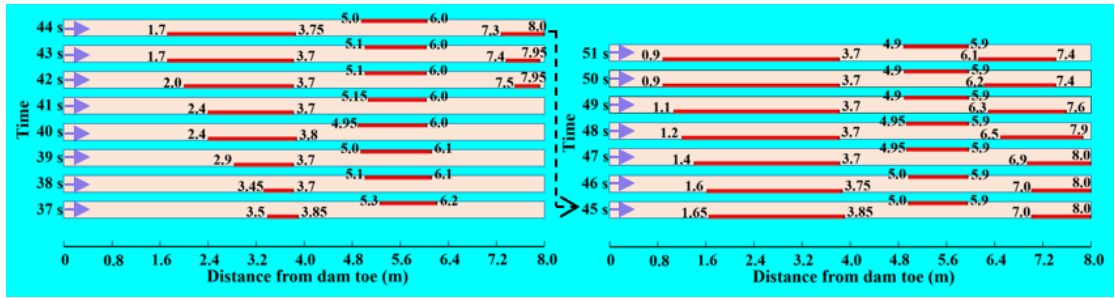
261

262

263

264

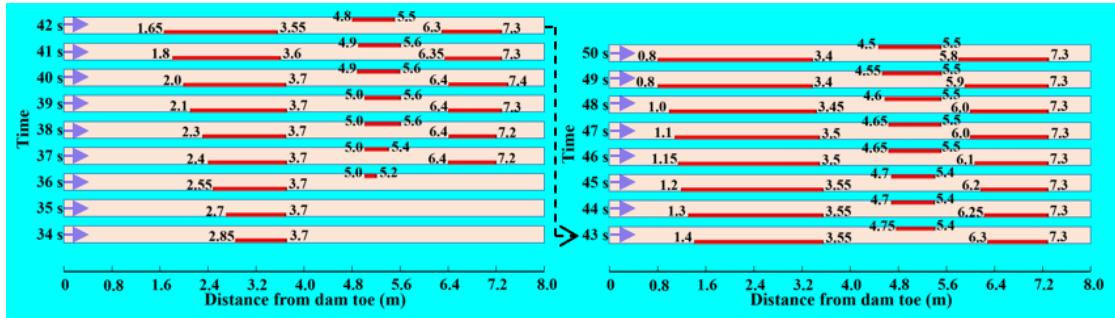
265



266

267

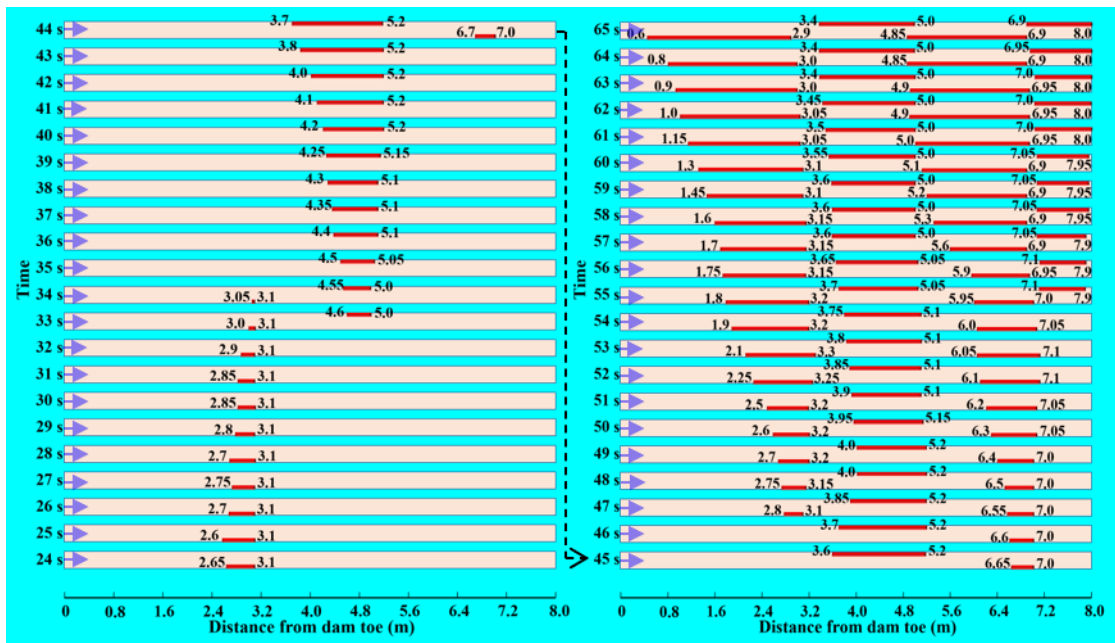
(d)



268

269

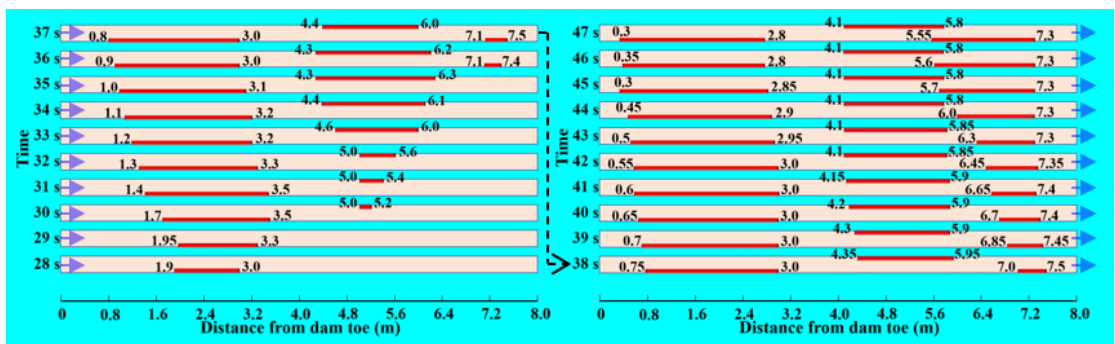
(e)



270

271

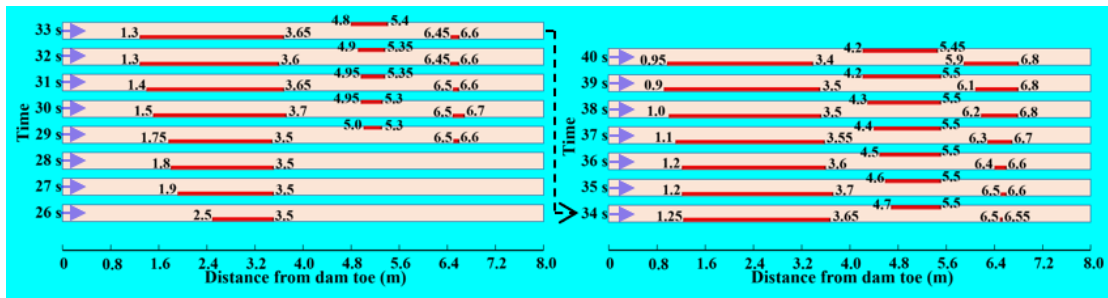
(f)



272

273

(g)



274

275

(h)

276 **Figure. 5.** The boulder bars' locations during the dam failure process. Notation: (a) to (h) represent  
 277 the boulder bars' locations for T1-T8 tests, respectively. The red lines in the figure represent the  
 278 boulder bars, and the orange rectangles represent the channels. **And, the purple arrow represents the**  
 279 **direction of flow.** The numbers at both ends of the red lines represent the distances between the  
 280 upstream and downstream edges of boulder bars and the dam toe.

281 The positions of the upstream edges of type II and III boulder bar moved toward  
 282 the dam toe during dam failure, but the downstream edges' positions could move toward  
 283 or away from the dam. The distances of movement of the downstream edge positions  
 284 were smaller than that of upstream edge positions. Compared with the boulder bars of  
 285 type I, the movements of type II and III boulder bars were smaller. The distance between  
 286 the boulder bars in the middle and downstream reaches is smaller than the distance  
 287 between boulder bars near the upstream reaches and adjacent boulder bars.

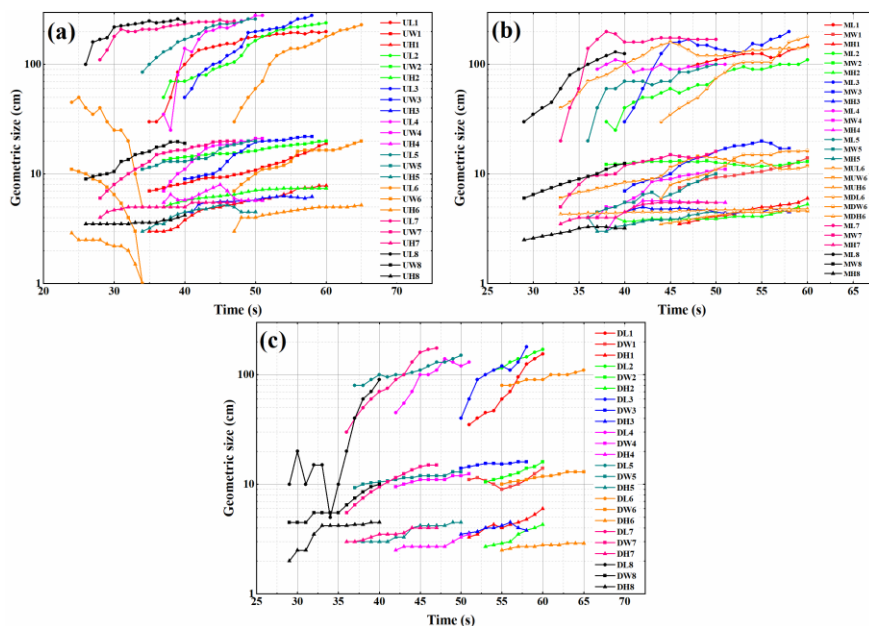
### 288 3.3 Geometry size of the boulder bar during dam failure process

289 It is corresponding to Sect. 3.2, Fig. 6 shows that the lengths of the boulder bars  
 290 of type I were longer than other types of boulder bars' lengths due to the sufficient  
 291 incoming materials from the upstream dam. For all the boulder bars, their lengths along



292 the channel were largest, followed by widths, and lastly the heights. Boulder bars'  
 293 lengths had a growing trend, and their growth rates were larger than widths and heights.

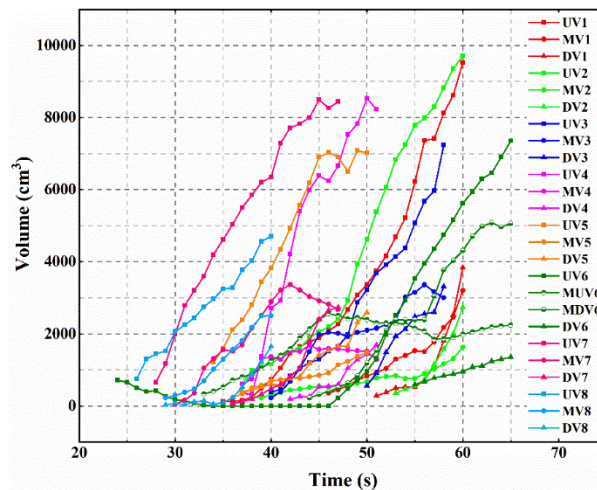
294 We recorded in detail the lengths, widths and heights of the boulder bars during  
 295 the dam failure process at each moment (Fig. 6). The figure shows that boulder bars'  
 296 heights changed less drastically than widths, which because boulder bars' heights were  
 297 significantly affected by outburst flow depth. In most cases, flow depth was less than  
 298 the heights of boulder bars. The sediments mainly accumulated at the boulder bars'  
 299 edges and middle and could not "climb up" boulder bars' tops. Besides, the reduction  
 300 of flow depth was not large enough, so the boulder bars' heights did not change seriously.  
 301 The boulder bars' widths were significantly affected by the discharge of the outburst  
 302 flow. When the discharge was enough, the sediments around the boulder bars were  
 303 taken away by the flow, and the widths decreased. The variations of widths and heights  
 304 both increase slowly with time and then tended to be stable values.



305  
 306 **Figure 6.** The lengths, widths, and heights of the boulder bars: (a) sizes of the boulder bars near  
 307 the upstream reaches; (b) sizes of the boulder bars near the middle reaches; (c) sizes of the boulder

308 bars near the downstream reaches. Notation: L, W, and H represent the length, width, and height of  
 309 the boulder bar, respectively.  $i$  represents the  $T_i$  experiment. For example, MUL6 indicates the  
 310 length of the boulder bar near the middle-upstream reaches for the T1 test.

311 When the amounts of sediments deposited on boulder bars were larger than the  
 312 quantities of eroded sediments, boulder bars' volumes became larger. Otherwise,  
 313 boulder bars' volumes would decrease or remain at a stable level. Figure. 7 reveals  
 314 boulder bars' volume characteristic during the dam failure. Most of the 25 boulder bars  
 315 gradually increased in volume, indicating that the amounts of outburst flow erosions in  
 316 the boulder bars' vicinities were less than the amounts of siltation during the entire  
 317 outburst process. Referred to Figs. 6 and 7, the boulder bars' volume characteristics  
 318 were consistent with the boulder bars' length characteristics. And because the widths  
 319 and heights developed slightly, boulder bars' volumes were mainly controlled by  
 320 boulder bars' lengths.



321  
 322 **Figure. 7.** Volumes of boulder bars. Notation:  $UV_i$ ,  $MV_i$ ,  $DV_i$ ,  $MUV_i$ ,  $MDV_i$  represent the volume  
 323 of the boulder bar near the upstream reaches, the boulder bar near the middle reaches, the boulder  
 324 bar near the downstream reaches, the boulder bar near the middle-upstream reaches, and the boulder

325 bar near the middle-downstream reaches, respectively. For example, UV1 means the volume of the  
326 boulder bar near the upstream reaches of the T1 test.

#### 327 **4. Geometry size of the boulder bars after dam failure**

328 In the Sec.3, we introduced formation characteristics and the geometry  
329 characteristics of the boulder bars during the dam failure processes. In this section, we  
330 will introduce the geometry characteristics of the boulder bar after the dam failure. After  
331 the dam failure, there were 25 boulder bars formed along the channel for all the tests.  
332 And it reflected the number of boulder bars was 0.4 to 1.0 times the ratio of river bed  
333 length to dam bottom length. The parameter  $R$  is defined as the ratio of boulder bar  
334 length  $L$  to width  $W$  in Eq. (1). And the dimensionless length  $L^*$  is calculated with Eq.  
335 (2), where  $L_d$  is dam bottom length.

336 Figure 8(a) shows the relationship between  $R$  and the  $L^*$  of the 25 boulder bars  
337 after the dams' failure in the experiments. The figure indicates that the values of  $R$  of  
338 the boulder bars all fell within the range of 8 to 14. And, the  $R$  increases with the  
339 increasing of  $L^*$ . However, the growth rate of  $R$  decreases as  $L^*$  goes by. The figures  
340 show that there is a hyperbola relationship between  $R$  and  $L^*$ . The hyperbolic function  
341 means that  $R$  would not sharply increase even become stable with the increasing of  $L^*$ .

$$R = \frac{L}{W} \quad (1)$$

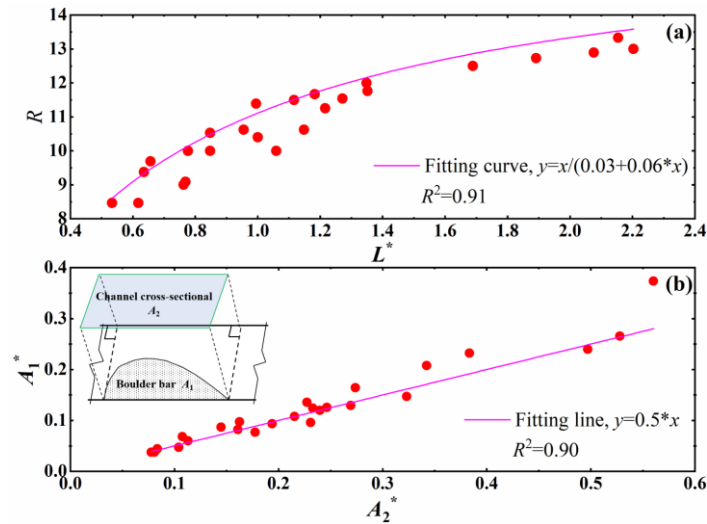
$$L^* = \frac{L}{L_d} \quad (2)$$

342 Two dimensionless parameters  $A_1^*$  and  $A_2^*$  are defined to reflect boulder bar's area

343 and channel cross-sectional area where the boulder bar located. They could be obtained  
 344 by Eqs. (2) and (3) respectively. The relationship between  $A_1^*$  and  $A_2^*$  is shown in Fig.  
 345 8(b). It can be seen that  $A_1^*$  increases as  $A_2^*$  increases. And there is a linear relationship  
 346 between  $A_1^*$  and  $A_2^*$ . The figure suggests that the ratio of boulder bar's area to river  
 347 channel cross-sectional area is approximately constant, which equals to 0.5.

$$A_1^* = \frac{A_1}{L_d^2} \quad (3)$$

$$A_2^* = \frac{A_2}{L_d^2} \quad (4)$$



348 **Figure.8.** Geometry characteristics of boulder bars after the dam failed in the experiments. (a)  
 349 the relationship between length to width ratio ( $R$ ) and dimensionless length ( $L^*$ ); (b) the relationship  
 350 between boulder bar's dimensionless area ( $A_1^*$ ) and the cross-sectional dimensionless area of the  
 351 river channel along the boulder bar ( $A_2^*$ ).

## 353 5. Discussion

354 In this paper, eight groups of landslide dam failure tests were conducted to

355 investigate the formation characteristics of boulder bars during the dam failure process,  
356 and the geometry characteristics of boulder bars during and after the dam failure, which  
357 are the main scientific objective of this paper. The experimental results are analyzed  
358 and explained to meet the scientific objective. It should be noted that the materials of  
359 riverbed and landslide dam were the same in the experiments. And the present  
360 experiments are limited to homogeneous riverbeds and dams.

361 In order to verify the results of the experiments, data of 38 boulder bars in filed  
362 formed by four landslide dam failures were used to compare the experimental data. It  
363 noticed that the data of boulder bars during the landslide dam failure process are still  
364 unavailable since the landslide dam mostly happened in inaccessible places and people  
365 could not get there to record the field data in time. Therefore, the filed data in this paper  
366 are all concerned about data after dam failure.

367 In this section, four field cases were used to verify the reliability of the boulder  
368 bar distribution and geometry characteristics in this paper. In the Fig.9, boulder bars  
369 were formed in the downstream river bed after Yigong landslide dam ( $30^{\circ}10'38.07''$  N,  
370  $94^{\circ}56'24.62''$  E), Tangjiashan landslide dam ( $31^{\circ}50'26.79''$  N,  $104^{\circ}25'51.17''$  E),  
371 Sedongpu landslide dam ( $29^{\circ}44'53.45''$  N,  $94^{\circ}56'24.02''$  E), and Hongshihe landslide  
372 dam ( $32^{\circ}36'16.05''$  N,  $105^{\circ}12'49.59''$  E) failed. The geometric data of boulder bars of  
373 the four cases were obtained from Google Earth. The length of the river bed section we  
374 selected was about 7 times of the dam bottom length. The detailed statistical data of  
375 boulder bars shown as Table 3. It indicates that the number of boulder bars on the 17  
376 km downstream river bed of the Yigong landslide dam was 2.67 times the ratio of the

377 river bed length to the dam bottom length; the number of boulder bars on the 5.6 km  
 378 downstream river bed of the Tangjiashan landslide dam was 1.29 times the ratio of the  
 379 river bed length to the dam bottom length; the number of boulder bars on the 6.4 km  
 380 downstream river bed of the Sedongpu landslide dam is 0.57 times the ratio of the river  
 381 bed length to the dam bottom length; and, the number of boulder bars on the 1.8 km  
 382 downstream river bed of the Hongshihe landslide dam was 1.29 times the ratio of the  
 383 river bed length to the dam bottom length. Generally, the number of boulder bars on the  
 384 river bed for the four field cases are 0.57 to 2.67 times the ratio of the river bed length  
 385 to the dam bottom length. These values are almost the same to the experimental values.

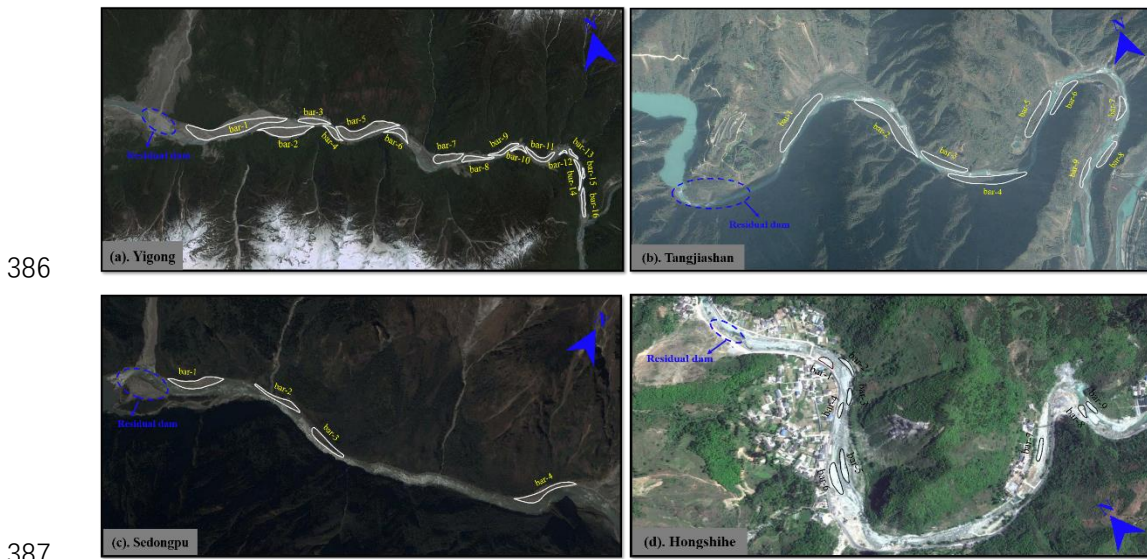


**Figure.9.** Google field images of four cases

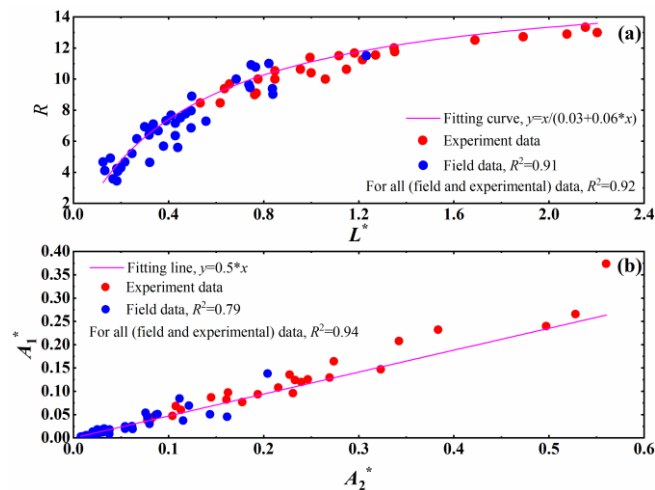
389 **Table 3** Field case data obtained through Google Earth.  $L_b$  is river bed length (m);  $L_d$  is dam bottom  
 390 length (m);  $N$  is the number of boulder bars (-);  $R$  is the ratio of boulder bar's length to width (-).

Case		Data				
Landslide dam	Boulder bar	$L_b$	$L_d$	$N$	$N/(L_b L_d^{-1})$	$R$
Yigong	bar-1	17	2.800	16	2.67	11.50
	bar-2					9.45
	bar-3					6.35
	bar-4					4.63

	bar-5					9.38
	bar-6					5.69
	bar-7					5.59
	bar-8					7.76
	bar-9					7.67
	bar-10					4.66
	bar-11					7.15
	bar-12					4.67
	bar-13					4.91
	bar-14					6.59
	bar-15					4.11
	bar-16					6.67
<b>Tangjiashan</b>	bar-1					10.00
	bar-2					11.00
	bar-3					8.89
	bar-4					10.91
	bar-5	5.6	0.803	9	1.29	6.86
	bar-6					7.96
	bar-7					5.21
	bar-8					6.40
	bar-9					7.11
<b>Sedongpu</b>	bar-1					9.64
	bar-2	6.4	0.914	4	0.57	10.77
	bar-3					7.29
	bar-4					9.03
<b>Hongshihe</b>	bar-1					4.23
	bar-2					6.92
	bar-3					4.29
	bar-4					4.06
	bar-5	2.1	0.300	9	1.29	7.31
	bar-6					7.50
	bar-7					6.15
	bar-8					3.44
	bar-9					3.57

391 In addition, we also analyzed the data about  $R$ ,  $L^*$ ,  $A_1^*$  and  $A_2^*$  of the field boulder  
392 bars. The Fig. 10(a) shows that the values of  $R$  of filed boulder bar all fall within the  
393 range of 2 to 12, which are approximate to the range of values of the experimental  
394 boulder bars. Furthermore, the hyperbola relationship in Fig. 8(a) is also suitable for  
395 the field data in Fig. 10(a). And, both the experimental and filed data points are all

396 closed to the fitting curve, whose coefficient of determination ( $R^2$ ) is 0.92. For the  
 397 boulder bars in the field,  $A_1^*$  and  $A_2^*$  show a linear relationship, and the fitting equation  
 398 of the experimental data (Fig.8 (b)) is very suitable for the field data in Fig.10 (b). It  
 399 means that the fitting line could predict the relationship between  $A_1^*$  and  $A_2^*$  for both  
 400 experimental and field boulder bar well (the coefficient of determination is 0.94).



401  
 402 **Figure.10.** Geometry characteristics of boulder bars after the dam failed in the field. The  
 403 experimental data are also plot in the figure to compare to the field data. (a) The relationship between  
 404 boulder bar length to width ratio ( $R$ ) and dimensionless length ( $L^*$ ); (b) The relationship between  
 405 boulder bar's dimensionless area ( $A_1^*$ ) and the cross-sectional dimensionless area of the river  
 406 channel along the boulder bar ( $A_2^*$ ).

407 Based on the above points, it can be seen that the experimental results in this paper  
 408 are consistent with the actual boulder bars in the field. Therefore, the experimental  
 409 results can provide references for the field study of the boulder bar formed by the  
 410 outburst flood triggered by landslide dam failure. The results in this paper can help  
 411 researchers deepen their understanding of river channel's geomorphological variation  
 412 characteristics affected by the outburst flood, and provide a data reference for the



413 analysis of the erosion and accumulation characteristics of the downstream river  
414 channel. Especially, with these two relationships, i.e.,  $R-L^*$  and  $A_1^*-A_2^*$ , the boulder bars  
415 geometry size could be predicated after a landslide dam formation in the future. Then  
416 the new landform after the dam failure could be evaluated. These presentations could  
417 contribute to the stream restoration planning, river navigation, and even utilization  
418 planning of the boulder bars.

## 419 **Conclusion**

420 In this paper, a downstream moveable bed for 4 to 7 times the length of landslide  
421 dam length along the channel was set, and through eight flume experiments, 25 boulder  
422 bars were formed downstream channel caused by overtopping flow. The boulder bar's  
423 formation process and geometry characteristics are studied. The main conclusions are  
424 as follows.

425 (1) Boulder bars first appear near dam toes (upstream reaches located on the dam's  
426 initial breach sides). Inertia force made sediment accumulate on the opposite banks of  
427 the channel bed, resulting in boulder bars' formations downstream. During the landslide  
428 dam failure process, the boulder bars' upstream edges are mainly in siltation states. The  
429 boulder bars' lengths increase with failure time, mainly caused by boulder bars'  
430 upstream edges move upstream. The downstream edges develop slowly and basically  
431 near the initial positions. And the developments of boulder bars' downstream edges are  
432 much smaller than the developments of boulder bars' upstream edges.

433 (2) During the dam failure process, the lengths varied faster than the widths and

434 heights of boulder bars. And the boulder bars' lengths along the river are the largest,  
435 followed by widths, and lastly the heights when the dam completed failed. The volumes  
436 of the boulder bars increase with dam failure, and boulder bars' volume characteristics  
437 are consistent with boulder bars' lengths characteristics.

438 (3) In the experiments, the ratio ( $R$ ) of boulder bar length to width falls at the range  
439 of 8 to 14. There is a nonlinearly relationship between length to width ratio ( $R$ ) and the  
440 dimensionless length of boulder bar ( $L^*$ ), which could be described as a hyperbolic  
441 equation. The dimensionless area ( $A_1^*$ ) of boulder bar has a linear relationship with the  
442 dimensionless area ( $A_2^*$ ) of the channel cross section, whose slope is about 0.5.

443 (4) In this paper, 38 boulder bars in the field triggered by four landslide dams'  
444 failures were investigated. By comparing the data of boulder bars in field with the  
445 boulder bars in the experiments, the distribution and geometric size characteristics of  
446 the boulder bars in the field are more consistent with the boulder bars in the experiments,  
447 indicating that the experimental results are more reliable.

#### 448 **Author contribution**

449 Xiangang Jiang was responsible for the experiments, article thinking, and writing.  
450 Haiguang Cheng was responsible for calculating the article parameters. Lei Gao was  
451 responsible for the article's pictures, and Weiming Liu was responsible for checking the  
452 full article.

#### 453 **Competing interests**

454 The authors declare that they have no known competing financial interests or

455 personal relationships that could have appeared to influence the work reported in this  
456 paper.

## 457 **Acknowledgments**

458 This research has been supported by The National Natural Science Foundation of  
459 China (No. 41807289) and Key Laboratory of Ministry of Education for Geomechanics  
460 and Embankment Engineering, Hohai University (No. 202020) and Open fund of Key  
461 Laboratory of mountain hazards and surface processes, Chinese Academy of Sciences  
462 (No. KLMHESP-20-05).

## 463 **Code and data availability statement**

464 The codes and data that support the findings of this study are available from the  
465 corresponding author upon reasonable request.

## 466 **Reference**

- 467 Ashworth, P. J.: Mid-channel bar growth and its relationship to local flow strength and  
468 direction, *Earth Surf. Process. Landforms*, 21, 103-123,  
469 [https://doi.org/10.1002/\(SICI\)1096-9837\(199602\)21:2<103::AID-  
470 ESP569>3.0.CO;2-O](https://doi.org/10.1002/(SICI)1096-9837(199602)21:2<103::AID-ESP569>3.0.CO;2-O), 1996.
- 471 Ashworth, P. J., Best, J. L., Roden, J. E., Bristow, C. S., and Klaassen, G. J.:  
472 Morphological evolution and dynamics of a large, sand braid-bar, Jamuna River,  
473 Bangladesh, *Sedimentology*, 47 (3), 533-555, [https://doi.org/10.1046/j.1365-  
474 3091.2000.00305.x](https://doi.org/10.1046/j.1365-3091.2000.00305.x), 2000.

475 Benito, G. and O'Connor, J. E.: Number and size of last glacial Missoula floods in the  
476 Columbia River valley between the Pesco Basin, Washington, and Portland,  
477 Oregon. Geological Society of America Bulletin, 115, 624 –638,  
478 [https://doi.org/10.1130/0016-7606\(2003\)115<0624:NASOLM>2.0.CO;2](https://doi.org/10.1130/0016-7606(2003)115<0624:NASOLM>2.0.CO;2), 2003.

479 Carling, P. A.: Freshwater megaflood sedimentation: what can we learn about generic  
480 processes? Earth-Science Reviews, 125, 87113,  
481 <https://doi.org/10.1016/j.earscirev.2013.06.002>, 2013.

482 Casagli, N., Ermini, L. and Rosati, G.: Determining grain size distribution of the  
483 material composing landslide dams in the Northern Apennines: Sampling and  
484 processing methods, Engineering Geology, 69, 83-97,  
485 [https://doi.org/10.1016/S0013-7952\(02\)00249-1](https://doi.org/10.1016/S0013-7952(02)00249-1), 2003.

486 Chen, S. C., Lin, T. W. and Chen, C. Y.: Modeling of natural dam failure modes and  
487 downstream riverbed morphological changes with different dam materials in a  
488 flume test, Engineering Geology, 188, 148-158,  
489 <https://doi.org/10.1016/j.enggeo.2015.01.016>, 2015.

490 Costa, J. E. and Schuster, R. L.: The formation and failure of natural dams, Geol Soc  
491 Am Bull, 100(7), 1054-1068, [https://doi.org/10.1130/0016-7606\(1988\)100<1054:TFAFON>2.3.CO;2](https://doi.org/10.1130/0016-7606(1988)100<1054:TFAFON>2.3.CO;2), 1988.

493 Jiang, X. G., and Wei, Y. W.: Natural dam breaching due to overtopping: effects of  
494 initial soil moisture, Bull Eng Geol Environ 78, 4821–4831,  
495 <https://doi.org/10.1007/s10064-018-01441-7>, 2018.

496 Jiang, X. G.: Laboratory Experiments on Breaching Characteristics of Natural Dams on

497 Sloping Beds, *Advances in Civil Engineering*, 5064093, 14,  
498 <https://doi.org/10.1155/2019/5064093>, 2019.

499 Jiang, X. G. and Wei, Y. W.: Erosion characteristics of outburst floods on channel beds  
500 under the conditions of different natural dam downstream slope angles, *Landslides*,  
501 1-12, <https://doi.org/10.1007/s10346-020-01381-y>, 2020.

502 Lamb, M. and Fonstad, M.: Rapid formation of a modern bedrock canyon by a single  
503 flood event. *Nature Geosci*, 3, 477 –481, <https://doi.org/10.1038/ngeo894>, 2010.

504 Maizels, J. K.: Jökulhlaup deposits in proglacial areas. *Quaternary Science Reviews*,  
505 16, 793 –819, [https://doi.org/10.1016/S0277-3791\(97\)00023-1](https://doi.org/10.1016/S0277-3791(97)00023-1), 1997.

506 Marren, P. M. and Schuh, M.: Criteria for identifying jökulhlaup deposits in the  
507 sedimentary record. In: Burr, D.M., Carling, P.A., Baker, V.R. (Eds.),  
508 *Megaflooding on Earth and Mars*, Cambridge University Press, 225-242,  
509 <https://doi.org/10.1017/CBO9780511635632>, 2009.

510 Mohrig, D., and Smith, J. D.: Predicting the migration rates of subaqueous dunes, *Water*  
511 *Resources Research*, 32 (10), 3207-3217, <https://doi.org/10.1029/96WR01129>,  
512 1996.

513 Morris, M. and Hassan, M., Kortenhaus, A., Geisenhainer, G., Visser, P.J., and Zhu,  
514 Y.: Modelling breach initiation and growth, Munich: HR Wallingford, 1(5):175-  
515 185, 2009.

516 Peng, M. and Zhang, L. M.: Breaching parameters of landslide dams, *Landslides*, 9, 1,  
517 13-31, <https://doi.org/10.1029/2018WR024107>, 2012.

518 Russell, A. J. and Knudsen, O.: Controls on the sedimentology of the November 1996  
519 jökulhlaup deposits, Skeiðarársandur, Iceland. In: Smith, N.D., Rogers, J. (Eds.),  
520 Fluvial sedimentology VI. Special Publication of the International Association of  
521 Sedimentologists, 28, 315 –329, <https://doi.org/10.1002/9781444304213.ch23>,  
522 1999.

523 Shaw, J. B., and McElroy, B.: Backwater number scaling of alluvial bed forms, J.  
524 Geophys. Res. Earth Surf, 121, 1436– 1455, doi:[10.1002/2016JF003861](https://doi.org/10.1002/2016JF003861), 2016.

525 Takahashi, T.: Debris flow Mechanics, Prediction and Countermeasures, Taylor and  
526 Francis Group, 35-38, <https://doi.org/10.1201/9780203946282>, 2007.

527 Turzewski, M. D., Huntington, K. W. and LeVeque, R. J.: The Geomorphic Impact of  
528 Outburst Floods: Integrating Observations and Numerical Simulations of the  
529 2000 Yigong Flood, Eastern Himalaya. Journal of Geophysical Research: Earth  
530 Surface, 124, 1056-1079, <https://doi.org/10.1029/2018JF004778>, 2019.

531 Wu C. H., Hu, K. H., Liu, W. M., Wang, H., Hu, X. D., and Zhang, X. P.: Morpho-  
532 sedimentary and stratigraphic characteristics of the 2000 Yigong River landslide  
533 dam outburst flood deposits, eastern Tibetan Plateau, Geomorphology, 107293,  
534 <https://doi.org/10.1016/j.geomorph.2020.107293>, 2020.

535 Zhou, G. G. D., Zhou, M. J., Shrestha, M. S., Song, D. R., Choi, C. E., Cui, K. F. E.,  
536 Peng, M., Shi, Z. M., Zhu, X. H., and Chen, H. Y.: Experimental investigation on  
537 the longitudinal evolution of landslide dam breaching and outburst floods,  
538 Geomorphology, 334, 29-43, <https://doi.org/10.1016/j.geomorph.2019.02.035>,  
539 2019.